The Astrophysical Journal Letters, 830:L33 (6pp), 2016 October 20 doi:10.3847/2041-8205/830/2/L33

SUNSPOT SIZES AND THE SOLAR CYCLE: ANALYSIS USING KODAIKANAL WHITE-LIGHT DIGITIZED DATA

Sudip Mandal[1] and Dipankar Banerjee[1,2]
[1] Indian Institute of Astrophysics, Koramangala, Bangalore 560034, India; sudip@iiap.res.in
[2] Center of Excellence in Space Sciences India, IISER Kolkata, Mohanpur 741246, West Bengal, India
Received 2016 September 23; revised 2016 October 5; accepted 2016 October 7; published 2016 October 20

ABSTRACT

Sizes of the sunspots vary widely during the progression of a solar cycle. Long-term variation studies of different sunspot sizes are key to better understand the underlying process of sunspot formation and their connection to the solar dynamo. The Kodaikanal white-light digitized archive provides daily sunspot observations for a period of 90 years (1921–2011). Using different size criteria on the detected individual sunspots, we have generated yearly averaged sunspot area time series for the full Sun as well as for the individual hemispheres. In this Letter, we have used the sunspot area values instead of sunspot numbers used in earlier studies. Analysis of these different time series show that different properties of the sunspot cycles depend on the sunspot sizes. The "odd–even rule" double peaks during the cycle maxima and the long-term periodicities in the area data are found to be present for specific sunspot sizes and are absent or not so prominent in other size ranges. Apart from that, we also find a range of periodicities in the asymmetry index that have a dependency on the sunspot sizes. These statistical differences in the different size ranges may indicate that a complex dynamo action is responsible for the generation and dynamics of sunspots with different sizes.

Key words: Sun: activity – Sun: oscillations – sunspots

1. INTRODUCTION

Sunspots are the cool and dark features visible in the solar photosphere. It has a strong periodic pattern, which is popularly known as the "solar cycle" or the "sunspot cycle," where the number of sunspots increase and decrease within 11 years. Apart from the prominent 11 year period, there are various short- and long-term periods present in the sunspot data. The "G–O rule" or the "odd–even rule" is one of them (Gnevyshev & Ohl 1948). According to this, the odd-numbered cycles are stronger compared to the preceding even-numbered one. This also sometimes leads to a periodicity of 22 years in the sunspot number data (Charbonneau 2010), which is the period of the solar magnetic cycle. There are other long-term periods such as the "Gleissberg cycle" with a period of ∼100 years.

Similar to the sunspot number, sunspot area also shows an 11 year period. In fact, in some cases, sunspot area is considered to be a better proxy than the sunspot number (Jordan & Garcia 2002). Sunspots come in different shapes and sizes, and the sunspot size depends on the solar cycle phase, i.e., larger spots mostly appear near the maximum of a given cycle (see Mandal et al. 2016). Independent sunspot observations, from different observatories, show that the sunspot areas follow a log-normal distribution (Bogdan et al. 1988; Baumann & Solanki 2005; Mandal et al. 2016). Cyclic variations of different sunspot sizes have been a study of great interest. Using Greenwich sunspot group number data, Javaraiah (2012, 2016) has shown the validation of the G–O rule and the Waldmeier effect for different sunspot group sizes. In an another work, using the same data, Obridko & Badalyan (2014) have shown different correlations between the cycle amplitudes for different set of sunspot sizes.

Using the Kodaikanal white-light digitized data, we construct different time series with different size scaling on the detected sunspots and investigate different properties of the solar cycle. Known properties of the sunspot cycle seem to hold for one range of sunspot sizes but not for all. In the following sections, we describe the data and method, followed by the results and a summary.

2. DATA DESCRIPTION AND METHOD

We use daily white-light sunspot observations, from 1921 to 2011, as recorded from the Kodaikanal observatory. In a recent initiative, the 90 years of the data have been digitized and calibrated, and the extraction of the sunspots, using a semi-automated method, has also been completed recently (Mandal et al. 2016, henceforth Paper I). Longitude, latitude, and the area (in the units of millionth of hemisphere, μHem) have been recorded for every detected sunspots. Using this information, different aspects of the solar cycle has been reproduced and presented in Paper I.

In this work, we isolate the sunspots into five different categories according to their sizes (S_a hereafter), defined as: $10\ \mu\text{Hem} \leqslant S_a < 50\ \mu\text{Hem}$, $50\ \mu\text{Hem} \leqslant S_a < 100\ \mu\text{Hem}$, $100\ \mu\text{Hem} \leqslant S_a < 200\ \mu\text{Hem}$, $200\ \mu\text{Hem} \leqslant S_a < 500\ \mu\text{Hem}$, and $S_a \geqslant 500\ \mu\text{Hem}$. These distributions are inspired from the size-resolved "butterfly diagram" as plotted in Figure 12 in Paper I. Two small and two large sunspot ranges are chosen in order to correctly identify the switchover size range for which we notice significant changes in the cycle properties. We did not choose thresholds higher than 500 μHem as the results will be statistically insignificant due to the lesser occurrences of "very large" sunspots (>1000 μHem) during a particular solar cycle. We use these thresholds in the daily sunspot data and compute the yearly averaged area values from that. Here, we emphasize the fact that due to different classification schemes in sunspot group identifications, the generated sunspot numbers seem to vary in different aspects (Clette et al. 2014; Dudok de Wit et al. 2016). Also, the use of sunspot area instead of the sunspot number has a distinct advantage in this case. Counting sunspot number gives equal weightage to every spot, whereas the area values are slightly weighted toward the large spots of the defined size range. Thus, in this paper, unlike the earlier

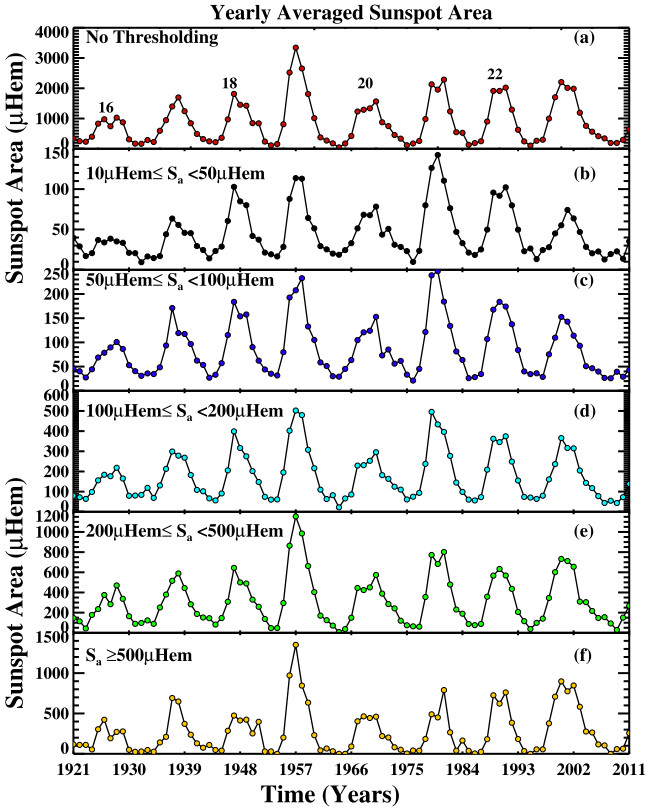

Figure 1. Yearly averaged sunspot area time series obtained for different sunspot sizes. Individual size ranges are noted on every panel.

studies, we have used the area criteria on the detected individual sunspots and calculated the total sunspot area for a particular day for the defined sunspot size range. This helps us explain the results more physically.

3. RESULTS

3.1. Odd–Even Rule and the Double Peaks

Different panels in Figure 1 show the yearly averaged sunspot area values for the period of 1921 to 2011, for different sunspot sizes. In Figure 1(a), we show area variations, for different cycles, as computed without any size restrictions. From the Figure 1(a) we notice that the odd-numbered cycles (cycles 17, 19, 21) have higher peak values compared to the preceding even-numbered cycles (cycles 16, 18, 20). This is in accordance with the odd–even cycle rule (Gnevyshev & Ohl 1948). For cycle 23, the increment is minimal compared to cycle 22. Now in Figure 1(b), we plot the yearly averaged variation for the smallest sunspot size range ($10\,\mu$ Hem $\leqslant S_a < 50\,\mu$Hem). Contrary to expectations, the small sunspots do not show any significant dependence on the overall cycle strengths. In this case, the highest peak corresponds to the 21st cycle, whereas the strongest cycle of the last century was the 19th cycle. Apart form that, cycle 18 and cycle 19 also show comparable strengths for this sunspot range, whereas the weaker cycles like cycle 16 and cycle 20 have relatively smaller peak heights. Also, we notice a clear violation of the odd–even rule, in the case of the smallest sunspots, for the 23rd cycle as its strength is significantly lower than the previous even-numbered 22nd cycle. This pattern persists for the next sunspot size range of $50\,\mu$Hem $\leqslant S_a < 100\,\mu$Hem as shown in Figure 1(c).

However, the scenario quickly changes as we move toward the mid-sized sunspot ranges (Figures 1(c), (d)). The cycle strength of the 21st cycle goes down and become comparable to 19th cycle as we move toward the largest-sized sunspots. Also, the amplitude difference between cycle 22 and cycle 23 becomes less. If we move further toward the largest-sized sunspots (Figure 1(f)), we see that the pattern matches very well with the "without thresholded" cycle variation as shown in Figure 1(a). We recover the "odd–even rule" again along with the cycle strengths. Thus, we see that the larger-size sunspot characteristics dominates in determining the overall cycle strengths.

Next, we focus on the occurrences of double peaks in the solar cycles during the maximum periods (Georgieva 2011) and their relation with the sunspot sizes. In Figure 1(a) we notice that for cycles 16, 21, and 22 there are clear signatures of double peaks. For cycles 20 and 23 there are also signature of double peaks but not as prominent as the other ones. Panels (b)–(f) in Figure 1 show that the occurrence of double peaks, for a particular cycle, is not a persistent signature in all the sunspot sizes. For example, we see a prominent double peak in cycle 21 (Figure 1(a)), which is present for the larger sunspot sizes (Figures 1(e), (f)) but absent for smaller sunspots. In a similar example, there is a weak double-peak signature for cycle 23 (Figure 1(a)), but for the largest size range ($S_a \geqslant 500\,\mu$Hem; Figure 1(f)) there is a prominent double peak. In fact, in most of the cycles, for the largest sunspot range ($S_a \geqslant 500\,\mu$Hem), we see a double peak near the time of sunspot maxima. Thus, we conclude that the double peaks in the solar cycle maxima occur for different sizes of the sunspots and there is no size bias, i.e., it may occur for small or large sunspots.

3.2. Long-term Variations

Apart from the 11 year and 22 year cycle periods, there are other long-term variations present in sunspot area data (Carbonell & Ballester 1990; Oliver et al. 1998; Krivova & Solanki 2002; Hathaway 2015). In order to probe this further, we use the yearly averaged sunspot area time series for different sunspot sizes. We summed the yearly averaged values for a particular cycle to produce a single number. It is thus a representation of the time-averaged strength of a particular cycle. In various panels in Figure 2, we show the same for different sunspot sizes. For the "no thresholding" case (Figure 2(a)) we do not see any new pattern apart from regular cycle strengths, i.e., the maximum bar height (referring to the amplitude) corresponds to 19th cycle and so on.

Now as we filter out the larger sunspots, i.e., only keeping the smaller sunspots (Figures 2(b), (c)), we see a clear pattern having a period of approximately of 10–12 cycles, i.e., 100–120 years. This period, in literature, is known as the Gleissberg cycle (Hathaway 2015), which represents the amplitude modulation of the 11 year cycle period. Furthermore, the obtained patterns in Figures 2(b) and (c) indicate that the cycle strength for the smaller sunspots will be progressively lower for cycle 24 and cycle 25.

As we go for larger sunspot sizes (Figures 2(d), (e)), we notice that the pattern with the ~100–120 year period disappears and the earlier trend flattens as we progressively move to larger sunspot sizes. Here, we also want to highlight

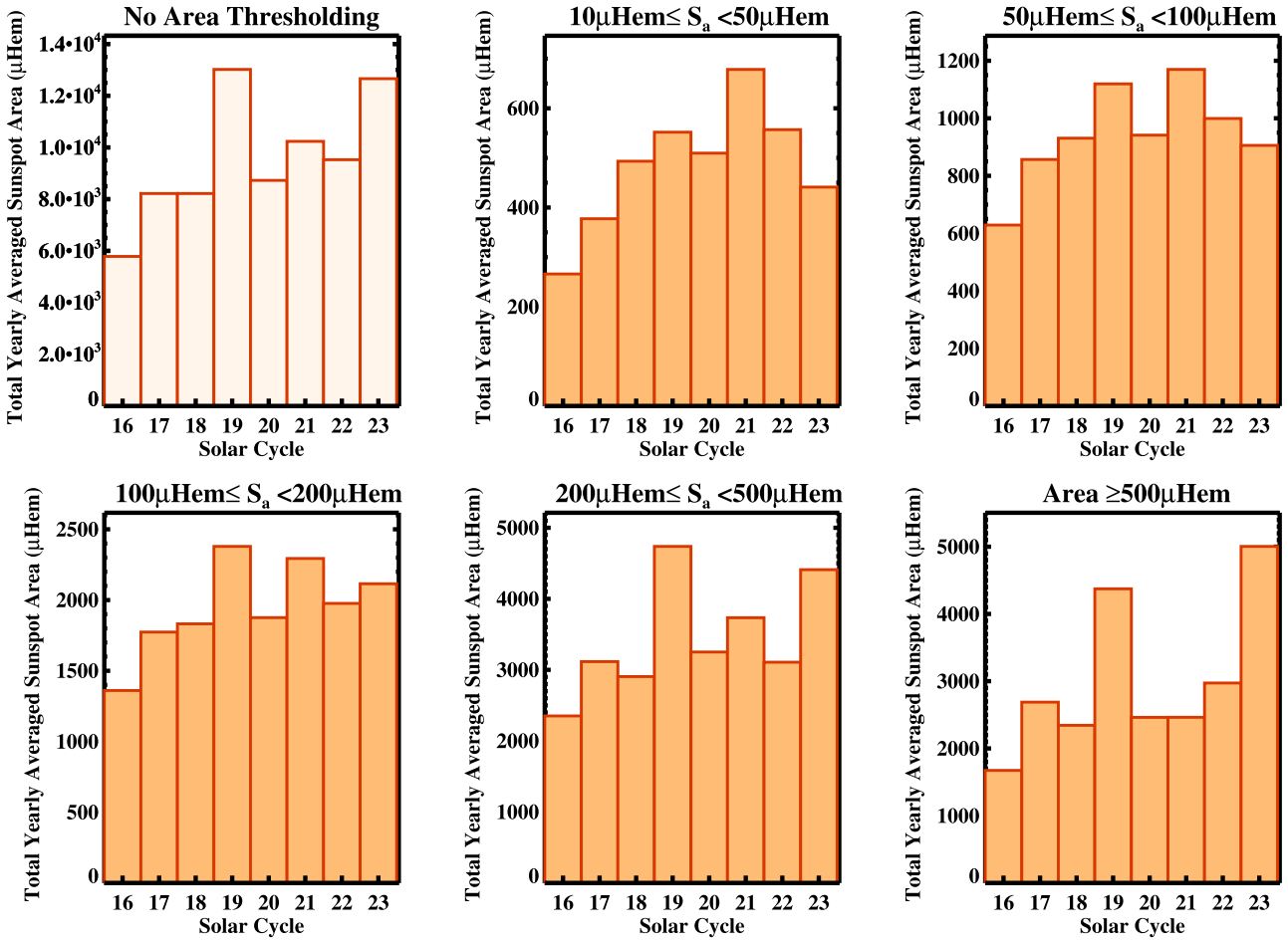

Figure 2. Variation of integrated cycle amplitudes with solar cycles. Each panel corresponds to a different sunspot size.

the fact that for the sunspot sizes 200 μHem $\leqslant S_a <$500 μHem, we notice that every odd cycle (cycles 17, 19, 21, 23) has a higher value compared to its immediate previous even cycle (cycles 16, 18, 20, 22). This is again the manifestation of the odd–even cycle rule, but for the integrated cycle amplitudes. For the sunspot size $S_a \geqslant 500$ μHem, the plot reveals something interesting. The height of the bar for the 23rd cycle is greater than that of the 19th cycle, i.e., the strength of the sunspots with highest sizes is more for the 23th cycle, whereas the overall cycle strength is less than that of the 19th cycle. This has happened due to extended occurrences of large sunspots during the prolonged decay phase of cycle 23 compared to cycle 19.

3.3. North–South Asymmetry

We know that the solar activities are not symmetric in both the hemispheres, and this hemispheric imbalance of the activities is known as "north–south asymmetry," or N–S asymmetry (Ballester et al. 2005; Temmer et al. 2006; Ravindra & Javaraiah 2015). Figure 3 shows the yearly averaged sunspot area variations for the two hemispheres, for the defined sunspot sizes. In Figure 3(a), we show the same for the "no thresholding" case. We notice a phase difference (lead or lag) between the two hemispheres, more prominently during the epoch of cycle maxima. Apart from that, we also see that the double peaks, for a given cycle, may occur for a particular hemisphere without having any counterpart of the same in the other hemisphere. As found earlier (Figure 1(f)), in this case also, most of the double peaks occur for the highest sunspot size range (Figure 3(f)).

Figures 3(b)–(f) show the hemispheric yearly sunspot for different sunspot sizes. A closer inspection reveals that for different sunspot sizes, one hemisphere dominates compared to the other and vice versa occurs for different size ranges. For example, for cycle 19, the northern hemisphere dominates over the southern for the small sunspots, whereas for the progressively larger sunspots the opposite behavior is seen, i.e., south dominates over north. In contrast, for cycle 22, the south dominates over the north for small sunspots, but gradually the difference minimizes as we reach toward larger sunspots. Though, we must emphasize that there are cycles for which we do not see any large change in the two hemispheres for any sunspot size range. Cycles 16, 17, and 23 are examples of such cases.

In order to quantify the asymmetry between the two hemispheres, we use the "north–south asymmetry index" ($A_{\rm ns}$) as $(S_{an}\text{-}S_{as})/(S_{an}+S_{as})$, where S_{an} and S_{as} are the yearly averaged sunspot area values for the northern and the southern hemispheres, respectively. We plot the time variation of $A_{\rm ns}$ for different sunspot sizes in different panels of Figure 4. At a first glance, we notice that the variation of $A_{\rm ns}$ is very smooth for the smallest sunspot sizes (Figure 4(b)), as compared to any other size range (Figures 4(c)–(f)). This can be understood from the definition of $A_{\rm ns}$, which varies between $\pm$1, depending upon

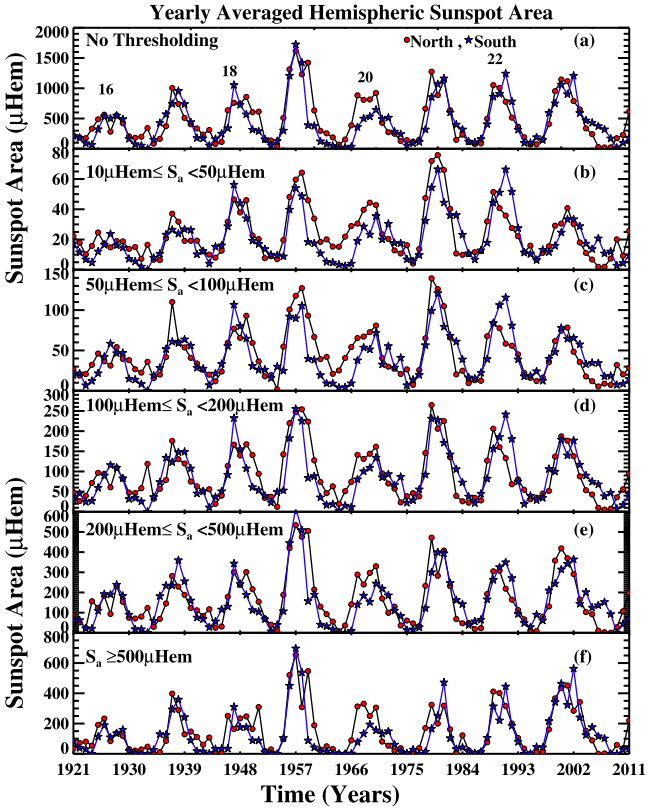

Figure 3. Yearly averaged hemispheric sunspot area for different sunspot sizes.

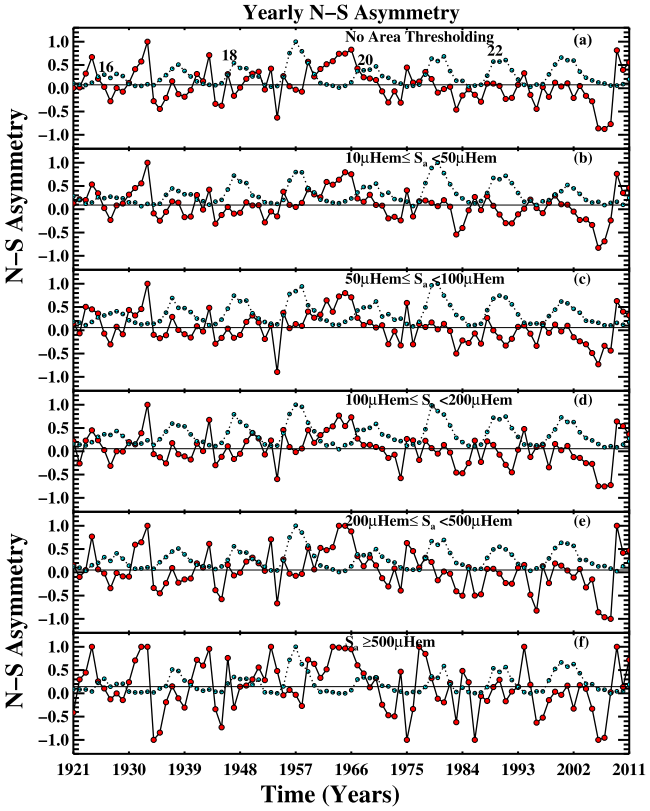

Figure 4. Time evolution of the asymmetry index, A_{ns}, for corresponding sunspot sizes.

the presence of at least one single sunspot in any of the hemispheres and absence of any spot in the other hemisphere. Since the smaller sunspots occur more frequently at the time of solar minima compared to the appearance of a large sunspot, the variation of A_{ns} is relatively smoother in the former case. We also notice (from Figure 4(a)) that at the maximum phase of cycle 21, A_{ns}, has values very close to zero as in the case of cycle 23. However, at the cycle 22 maximum, A_{ns} attains a maximum value of ≈ -0.5. This is consistent with the results as obtained by Javaraiah (2005). This scenario changes a little as we move from small to large sunspot sizes. There is a hint of long-term variation in the asymmetry index. For the largest-sized sunspots (Figure 4(f)), the northern hemisphere dominates in the cycle minima until cycle 20, after which the southern hemisphere dominates. This trend is also visible in Figure 4(e).

3.3.1. Periodicities in the N–S Asymmetry

Since the solar cycle has a dominant period of 11 years, it is expected that the N–S asymmetry index will also have some periodicity. There has been a lot of work done in order to probe this periodicity (Carbonell et al. 1993; Ballester et al. 2005; Chang 2009; Javaraiah 2015; Ravindra & Javaraiah 2015). Here, we revisit the periodicity in the N–S asymmetry for different sunspot sizes.

We use the A_{ns} curves, shown in different panels in Figure 4, and the wavelet analysis in order to obtain the periodicities in A_{ns}. Results of the wavelet analysis on the different A_{ns} curves is shown in Figure 5. The global wavelet power (time-averaged power as shown in the "wavelet power spectrum panel") is calculated along with a significance level of 90%. This significance level is obtained for the white noise (Torrence & Compo 1998), and contours are overplotted on top of the wavelet spectrum in order to highlight the region above the confidence level. In the global wavelet panel, a horizontal dashed line indicates the maximum measurable period due to the "cone of influence" (COI; which arises due to the edge effect and is represented by the cross-hatched region marked in the wavelet power spectrum panel).

The top panel of Figure 5 shows the period obtained from the "no thresholding" case where we see that the dominant period is 16.5 years (Javaraiah 2015) and the second-highest period is 9 years (Chang 2009). Wavelet spectrum and the corresponding periods obtained for different sunspot sizes are shown in consecutive panels in Figure 5. We notice that the dominant periods for the small sunspot sizes (sizes from $10\ \mu\text{Hem} \leqslant S_a < 100\ \mu\text{Hem}$), are 10.7 years, 11.7 years (Carbonell et al. 1993), and 16.5 years. Now as we move toward larger-sized sunspots ($100\ \mu\text{Hem} \leqslant S_a < 500\ \mu\text{Hem}$), shorter periodicities are observed to appear. Apart form the 10.7 years and 16.5 years, we now have periodicities of 8.3 and 5.4 years. For the largest-sized sunspots ($\geqslant 500\ \mu$Hem), we even get as small a period as 4.9 years apart from the dominant 11.7 years. We also see that there are two other periods at ~30 years and ~46 years present for different sunspot sizes. However, these two periods are beyond the faithful detection level determined by the COI (this arises due to the duration of the time series). Though, it is worth mentioning here that a period of $\approx$44 years, double that of the solar magnetic cycle, has been reported earlier from the N–S asymmetry (Ballester et al. 2005).

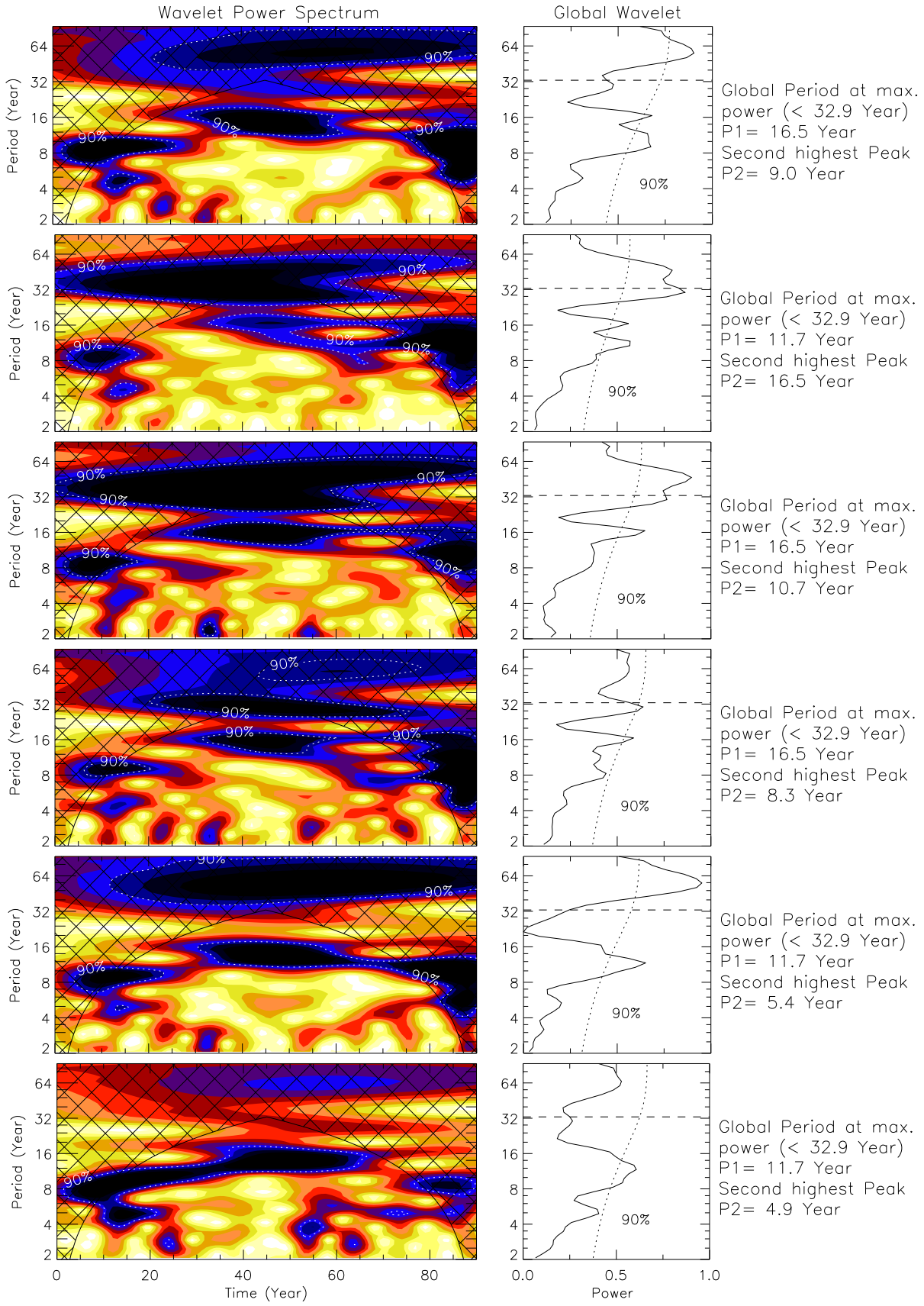

Figure 5. (Top to bottom) Results of the wavelet analysis corresponding to the light curves of A_{ns}, as shown in Figures 4(a)–(f), respectively. The periods with the maximum significant powers are listed after the wavelet power spectrum (left panel) and the global wavelet plot (middle panel).

4. SUMMARY AND CONCLUSIONS

Different sunspot sizes manifest different distinct properties on shorter and longer timescales compared to the dominant 11 year period. In our analysis, we have used sunspot area values, which turn out to be a better proxy than sunspot number for this type of studies. Below, we summarize the main results found from the analysis:

1. Our analysis shows that the overall pattern of a cycle is primarily dictated by the larger-size sunspots. Small-sized sunspots show no clear correlation with the overall cycle strengths. We found cycle 21 to be the strongest cycle considering the small sunspots only. At the same time, we notice that, for this cycle, the cycle strength considering the large spots decreases gradually. This is also true for cycle 18 and cycle 22. For the 19th cycle, the case gets reversed. Thus, this supports the idea of a dynamo mechanism where small sunspots are the fragmented part of the larger sunspots.
2. For cycle 23, the odd–even rule gets violated, particularly for the small-sized sunspots. However, for the larger spots, the anomaly seems to reduce. Also, the double peaks at the solar maxima are not found in all the sunspot sizes. Though not prominent, the trend shows that the occurrence of double peaks is maximum for the largest sunspot sizes, whereas occasionally it shows up for the small sunspots.
3. A clear pattern of a ∼120–130 year period has been found for the small sunspot sizes. The observed trend also implies that the cycle strengths of cycle 24 and cycle 25, for the small sunspot, will be weaker than that of cycle 23. Here, we notice that the pattern disappears for the large sunspots indicating that on a long-term basis (longer than the 11 year period) the two size scales also have two different trends.
4. Hemispheric asymmetry is found to be different for different sunspot sizes. The double-peak behavior, for a particular cycle, also shows a hemispheric dependence. Analyzing the asymmetry index (A_{ns}) times series, we found dominant periods of 9 years, ≈12 years, and 16.5 years in most of the sunspot sizes. Apart form that, we obtained smaller periods like 8.3 years, 5.4 years, and 4.9 years for the larger-sized sunspots. The presence of periods ≈5 years can be a manifestation of the asymmetric nature of the solar cycle.

There is currently no understanding of the physical reason for a possible sunspot size dependence on the solar dynamo. Sunspot area distributions, for the large and the small sunspot sizes, have been found to be distinctively different (Bogdan et al. 1988). Results from our analysis also indicate such anomalies for large and small sunspots. We thus conjecture that these phenomena can be explained by a dynamo formulation with two components, one directly connected to the global component of the dynamo (and the generation of bipolar active regions), and the other with the small-scale component of the dynamo (and the fragmentation of magnetic structures due to their interaction with turbulent convection; Muñoz-Jaramillo et al. 2015).

To conclude, we have analyzed daily sunspot data, obtained from Kodaikanal, in order to investigate the sunspot size dependence of various solar cycle features. We found distinct signatures present for the small-, medium-, and large-sized sunspot area time series that may indicate a complex dynamo operating differently on different size scales. Independent studies using other solar proxies and other data sets will help us to understand the underlying mechanism responsible for these phenomena.

The authors would like to thank the referee for valuable suggestions that helped with a better presentation of the paper. We would also like to thank the Kodaikanal facility of Indian Institute of Astrophysics, Bangalore, India for proving the data. The data series is now available for public use at http://kso.iiap.res.in/data.

REFERENCES

Ballester, J. L., Oliver, R., & Carbonell, M. 2005, A&A, 431, L5 Baumann, I., & Solanki, S. K. 2005, A&A, 443, 1061
Bogdan, T. J., Gilman, P. A., Lerche, I., & Howard, R. 1988, ApJ, 327, 451
Carbonell, M., & Ballester, J. L. 1990, A&A, 238, 377
Carbonell, M., Oliver, R., & Ballester, J. L. 1993, A&A, 274, 497
Chang, H.-Y. 2009, NewA, 14, 133
Charbonneau, P. 2010, LRSP, 7, 3
Clette, F., Svalgaard, L., Vaquero, J. M., & Cliver, E. W. 2014, SSRv, 186, 35
Dudok de Wit, T., Lefèvre, L., & Clette, F. 2016, SoPh, in press (doi:10.1007/s11207-016-0970-6)
Georgieva, K. 2011, ISRAA, 2011, 437838
Gnevyshev, M. N., & Ohl, A. I. 1948, AZh, 25, 18
Hathaway, D. H. 2015, LRSP, 12, 4
Javaraiah, J. 2005, MNRAS, 362, 1311
Javaraiah, J. 2012, SoPh, 281, 827
Javaraiah, J. 2015, NewA, 34, 54
Javaraiah, J. 2016, Ap&SS, 361, 208
Jordan, S. D., & Garcia, A. G. 2002, in BAAS, 34, 737
Krivova, N. A., & Solanki, S. K. 2002, A&A, 394, 701
Mandal, S., Hegde, M., Samanta, T., et al. 2016, A&A, submitted (arXiv:1608.04665)
Muñoz-Jaramillo, A., et al. 2015, ApJ, 800, 48
Obridko, V. N., & Badalyan, O. G. 2014, ARep, 58, 936
Oliver, R., Ballester, J. L., & Baudin, F. 1998, Natur, 394, 552
Ravindra, B., & Javaraiah, J. 2015, NewA, 39, 55
Temmer, M., Rybák, J., Bendík, P., et al. 2006, A&A, 447, 735
Torrence, C., & Compo, G. P. 1998, BAMS, 79, 61